

## Effect of uniform magnetic field on dose distribution in the breast radiotherapy

A.D. Esmaeeli<sup>1\*</sup>, M. Pouladian<sup>1</sup>, A.S. Monfared<sup>2</sup>, S.R. Mahdavi<sup>3</sup>,  
D. Moslemi<sup>4</sup>

<sup>1</sup>Department of Medical Radiation Engineering, Science and Research Branch, Islamic Azad University, Tehran, Iran

<sup>2</sup>Department of Medical Physics, Babol University of Medical Sciences, Babol, Iran

<sup>3</sup>Department of Medical Physics, Tehran University of Medical Sciences, Tehran, Iran

<sup>4</sup>Department of Radiation Oncology, Babol University of Medical Sciences, Babol, Iran

### ABSTRACT

**Background:** To reduce the dose to normal tissues surrounding the treated breast, a uniform magnetic field was used within a humanoid phantom in breast radiotherapy. **Materials and Methods:** Monte Carlo simulations were performed with GEANT4, irradiating humanoid phantoms in a magnetic field. To reconstruct phantoms, computed tomography (CT) data slices of four patients were used for the Monte Carlo simulations. All of them had left breast cancer either or not mastectomy. In the simulations, the planning and methods of chest wall irradiation were similar to the actual clinical planning. **Results:** Utilizing magnetic field will help to produce uniform dose distribution to the breast with a sharp dose-volume histogram (DVH) curve for the planning target volume (PTV), however, for the ipsilateral lung and chest wall skin the mean dose was reduced by a mean of 16% and 12% at 1.5 T, and 9% and 7% at 3 T, respectively. The magnetic field was shown to restrict the lateral spread of secondary electrons to the contralateral organs, resulting in significant dose reductions to the contralateral breast (CB) and contralateral chest wall skin (CCWS) by a mean (range) of 28% (21-37%) and 58% (44-75%) at 1.5 T, and 48% (32-81) and 66% (54-73%) at 3 T, respectively. **Conclusion:** The simulations established that the magnetic field can reduce the dose to the internal and contralateral tissues and increase it to the PTV with sharper edge DVH curve.

**Keywords:** ERE, magnetic field, breast, GEANT4.

### ► Original article

**\* Corresponding author:**

Dr. Ali Esmaeeli Dafchahi,

Fax: +98 131 4247056

**E-mail:**

[ali\\_esmaeeli\\_d@yahoo.com](mailto:ali_esmaeeli_d@yahoo.com)

Received: Jan. 2013

Accepted: April 2013

*Int. J. Radiat. Res.*, April 2014;  
12(2): 151-160

### INTRODUCTION

It is well known that radiation is a carcinogen; therefore, it is very importance to reduce exposure to normal tissues while maximizing the dose to the targeted area (s). It is this principle of minimizing unwanted dose that has prompted many studies in the reduction of exposure to the internal and contralateral breast. However, delivering too high a dose will cause complications to normal tissues including

radiation-induced pneumonitis, cardiac toxicity, secondary cancers and skin reactions. The probability of occurring of such effects depends primarily on the delivered dose and the volume of the received dose. Boice *et al.* (1992) <sup>(1)</sup> found a correlation between the amount of dose to the contralateral breast and the likelihood of a secondary malignancy formation.

Multiple groups have proposed designs for reducing the dose to the internal and contralateral organs; for example, choosing a radiation technique like breast intensity

modulated radiotherapy (IMRT), 3-dimensional conformal radiotherapy (3D-CRT), partial breast radiotherapy and high-dose rate (HDR) brachytherapy or using a platform-based breast shield that minimizes exposure of internal organs<sup>(2-7)</sup>.

Many studies have proposed designs for combining a linear accelerator (Linac) or a <sup>60</sup>Co tele-therapy unit with a magnetic resonance imaging (MRI) system for taking the real-time image guidance along with the treatment<sup>(8-19)</sup>. Furthermore, other studies have considered the possibility of using a magnetic field in a variety of geometries in order to investigate perturbations on dose distributions to improve volumetric conformance in radiotherapy<sup>(9,20-23)</sup>. The consequences of a magnetic field on dosimetry have been studied by all of these groups using analytical, Monte Carlo (MC) and/or experimental techniques. Largely, the focus has been on changes to the spatial distribution of dose resulting from the magnetic field influence on charged particle transport. They have established that high magnetic field strength can have significant perturbations on dose distributions, such as changes to the percentage depth dose, tissue interface effects (electron return effect) and lateral shifts in dose distributions in the photon beam radiotherapy<sup>(17,24-26)</sup>. These effects are most noticeable in the tissue-lung interface where the field passes through the interface<sup>(13,17,25)</sup>.

The aim of this work was to investigate the consequences to radiation dose distributions that occur in different magnetic field strengths in order to understand any advantages it may provide in comparison with the zero magnetic field in breast radiotherapy. Possible advantages could be uniformed dose to the treated volume and decreased dose to the internal and contralateral breast organs.

## **MATERIALS AND METHODS**

### **Monte Carlo simulations**

The MC toolkit GEANT4 (v9.3) has been used to calculate the dose distribution in a reconstructed patient-derived phantom in the

presence of a magnetic field. GEANT4 is a multipurpose MC code, developed and maintained by the GEANT4 collaboration<sup>(27)</sup>.

All regular physical processes for medical applications from the LowEPhysics Processes package were actuated. The low-energy cut-offs for different materials used in this work were considered according to default values which were defined in GEANT4<sup>(31)</sup>. The human body tissues like lung, liver, chest wall, bones were modeled according to the International Commission on Radiation Units and measurements (ICRU) report 46<sup>(32)</sup>.

For the calculation of the trajectories of charged particles in a magnetic field, the method 'ClassicalRK4' was used (for more information see GEANT4.9.3 user's guide for application developers). This code was shown to provide accurate results for gamma ray dose distributions in the presence of a magnetic field<sup>(29)</sup>. The simulations were performed 20 times with independently created phase-space files. From the resulting dose distributions, an averaged dose profile and a standard deviation profile were obtained. The chosen number of particles ensured a statistical uncertainty of 1%, 1 SD (for all voxels with the dose of more than 1% of maximum dose).

### **Target anatomy and treatment planning setups**

In this work, we have chosen four patients who had breast cancer with mastectomy and non-mastectomy cases. Breast treatment plan setups were tabulated in table 1, and the PTV and organs at risk (OARs) together with wedges and treatment beam directions were shown in figure 1(a). The external surface of patients and lung contours were defined by automated density gradient tracking; then, they were edited and verified by physicians. The PTV was defined by adding 5 mm to the clinical target volume (CTV). The contour of the PTV was outlined with depth of 1.6 mm to the skin surface anteriorly to evaluate DVHs. To assess the value of skin dose accurately, another volume including 1.6 mm surface thickness of the CTV was contoured as the skin structure.

**Table 1.** Treatment plan setups and patient specifications.

Treatment plan parameters	Patient # 1		Patient # 2		Patient # 3		Patient # 4	
	Beam 1 (Medial)	Beam 2 (Lateral)						
SSD <sup>a</sup> (cm)	90.5	90.8	94.6	94.5	92.6	93.3	93.3	93.3
Collimator Width (cm)	9.6	9.6	6.4	6.4	7.6	7.6	9.8	9.8
Collimator Length (cm)	22.0	22.0	22.4	22.4	21.0	21.0	20.6	20.6
Gantry Angle (degree)	305	131	305	128.5	297	121	295	121
Wedge (degree)	30	30	15	15	15	15	15	15
Mastectomy/age/BMI <sup>b</sup>	No/42/32		Yes/59/27		Yes/45/24		No/44/35	
LOD <sup>c</sup> (cm)	1.4		0.7		2.8		1.8	

<sup>a</sup> Source to Surface Distance

<sup>b</sup> Body Mass Index

<sup>c</sup> Lung Orthogonal Distance: is defined as the maximum breast and lung distance (see figure 1 (a)).

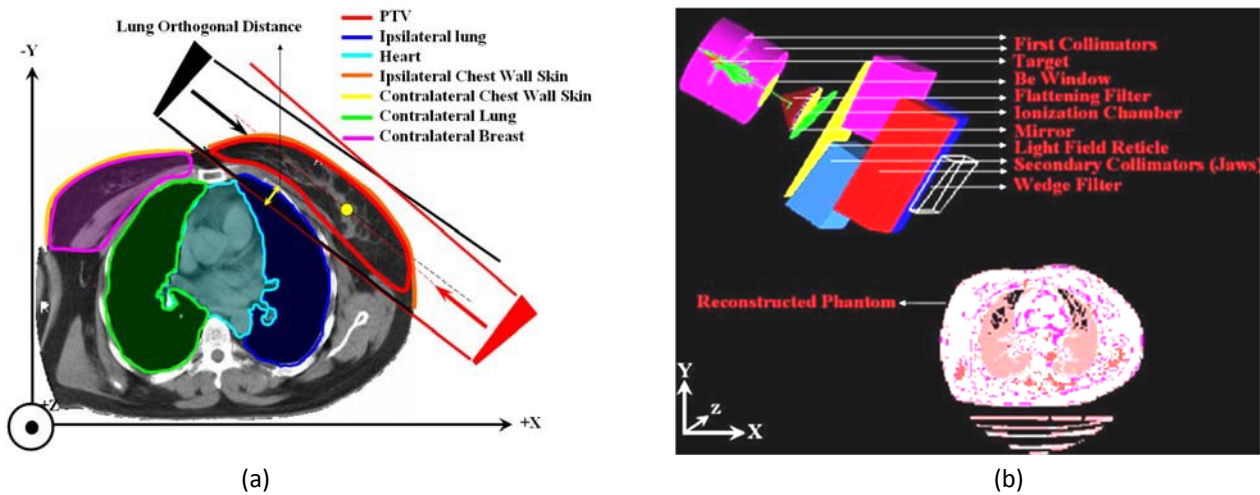


**Figure 1.** (a) Target anatomy and structure, OARs, medial and lateral beams, and lung orthogonal distance in patient # 1. (b) One slice of the reconstructed phantom (patient # 1) along with Linac head simulated in GEANT4.

CT data slices of each patient were used in the MC code as input data. Dimensions of each voxel in the reconstructed image of patients in GEANT4 were  $0.8 \times 0.8 \times 3 \text{ mm}^3$ . One slice of the reconstructed phantom (patient # 1) and the path of the medial beam together with Linac head setups simulated in GEANT4 were presented in figure 1(b). In the simulations, the planning and methods of chest wall irradiation were similar to the actual clinical planning. The treatment planning system (TPS) used in this study is the TiGRT TPS, External Treatment Planning version 1.0.140.5061.L1.244584 (LinaTech, LLC, Sunnyvale, CA, 94086). This TPS software uses super-position convolution algorithm to calculate the dose distribution. Commissioning and verification under experimental condition are done with TiGRT

TPS. Plan files, including CT data, were exported from the TPS and imported into GEANT4 for MC simulation.

In the simulations, a global magnetic field was implemented in the x direction (figure 2). Unidirectional photons with a realistic 6 MV linear accelerator energy were used as a source that was previously compared with a real Linac (Siemens Primus) in the water phantom (30). All voxels were placed as parameterized volumes on a background material of air.

Different components of the simulated linear accelerator (Siemens Primus) for a 6-MV photon beam were shown in figure 1(b). For each beam, a phase space was generated below the wedge and without the presence of any magnetic field. The assumption implicit in this model was that the B0 field was negligible to this point due to

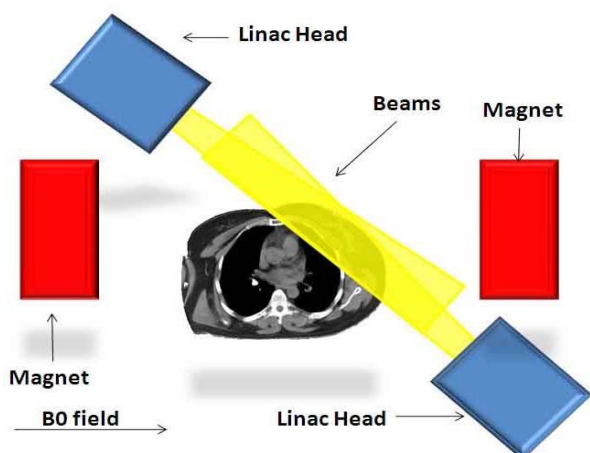


**Figure 2.** Schematic representation of the magnetic field geometry for the medial and lateral beams, showing relative positioning of the Linac, magnets and the magnetic field direction.

the magnetic shielding implicit in the Linac-magnetic resonance design. The contaminant electrons were included in the present phase-space data. Each phase space was then used as a source in the GEANT4 platform. It should be noted that, the contaminant electrons were thus subjected to the magnetic field from this point on in this model.

In order to verify the Linac head along with the wedge and treatment plan setups in the GEANT4 MC code, dose distributions calculated by the MC simulations were evaluated using dose distributions calculated by the TPS by comparing DVHs of the PTV, ipsilateral lung (IL) and heart volumes.

Two opposed parallel beams described as being tangential to the chest wall were implemented. Each beam was simulated separately and the results were combined and normalized to 100% at isocenter for the zero field case. Absolute dose can be obtained by multiplying all voxel doses by the dose-to isocenter/100% for the zero field plan. The nominal prescribed dose was 50 Gy in 25 fractions using 6-MV photons. The calculated dose was normalized to a relevant point in the PTV to provide dose homogeneity. The mean dose of each organ was normalized to mean dose of PTV at 0 T.

The mean dose, DVHs and dose-area histograms (DAHs) obtained for the PTV, heart,

IL, contralateral lung (CL), ipsilateral chest wall skin (ICWS), CCWS and CB in humanoid phantoms were considered for investigating the effect of the magnetic field on the dose distribution to the internal and contralateral organs.

## RESULTS AND DISCUSSION

### Comparison of the MC and TPS

Comparisons of the DVHs for the MC and TPS in the case of 6 MV breast patients were shown in figure 3. The PTV dose calculation evaluations showed a good comparison with the MC simulations and TPS. Table 2 demonstrates mean dose values calculated by the TPS and GEANT4. Comparisons of the mean dose for the TPS and GEANT4 showed deviations in the order of 5% maximum.

### Dose distribution to the ipsilateral organs

To illustrate differences in the relative dose distribution, results of the simulations were presented for different magnetic fields with respect to the zero magnetic field in the middle slice of the central plane for patients in figure 4. Figure 5 depicts the corresponding difference maps of figure 4 from the zero magnetic field case. Dose distributions to the breast and lung were nearly uniform at 0 T; but, at 1.5 and 3 T, sharp regions were produced at breast-lung boundaries (figure 4). This is explained by the fact that when photon beams irradiate without a magnetic field, charged particles travel into a chest wall and this process produces a large number of electrons in a predominantly forward direction. Dose deposition arises from these electrons along their path. In the presence of the magnetic field, electron trajectories are bent,

**Table 2.** Mean organ dose calculated by the TPS and MC.

Organ	Mean Dose (Gy)							
	Patient # 1		Patient # 2		Patient # 3		Patient # 4	
	MC	TPS	MC	TPS	MC	TPS	MC	TPS
PTV	49.4	50.0	50.5	50.0	50.0	50.0	50.0	50.0
IL	7.4	7.5	3.7	3.8	7.8	8.2	3.4	3.5
Heart	2.8	2.7	2.8	2.7	6.0	5.7	1.4	1.3

describing a helical path. In the chest wall, the mean free path length is short in comparison to the spiral radius. However, as soon as the electrons leave the chest wall and enter into the low-density media, like lung, their length of mean free path gets longer compared to their helical radius. Therefore, the helical path can be followed by small interaction and the electron will re-enter the chest wall. This will happen regardless of the exit angle of the electrons. Therefore effectively all electrons return into the

chest wall. This phenomenon is called the electron return effect (ERE) (25), which causes dose reduction in low-density media close to the dense ones.

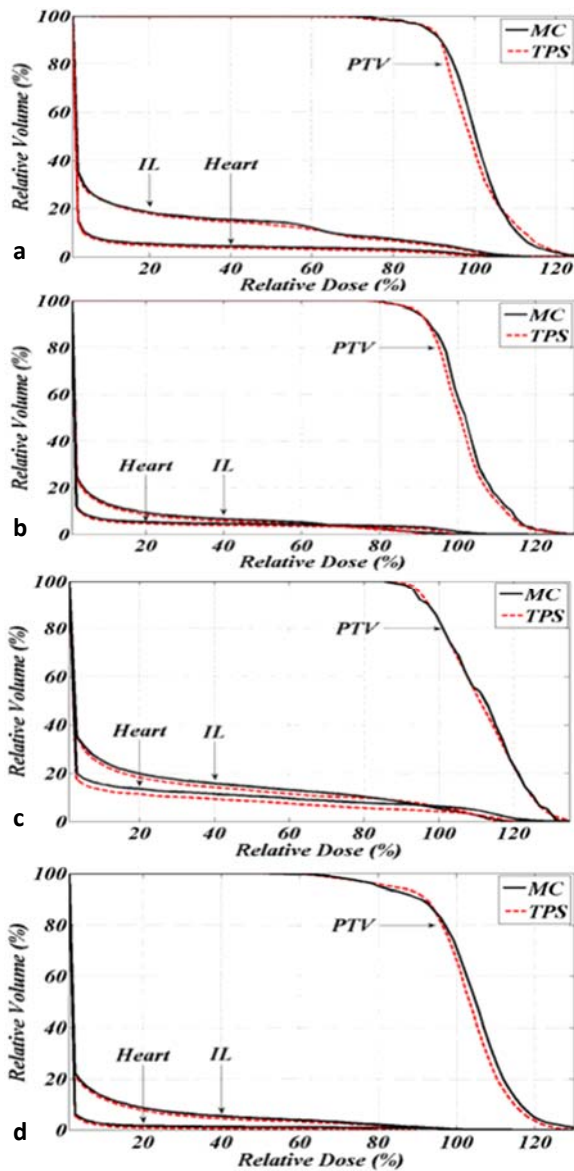


**Figure 3.** DVHs of the PTV, IL and heart for comparison of the TPS and MC calculated dose distributions in the 6MV breast case for (a) patient # 1, (b) patient # 2, (c) patient # 3 and (d) patient # 4.

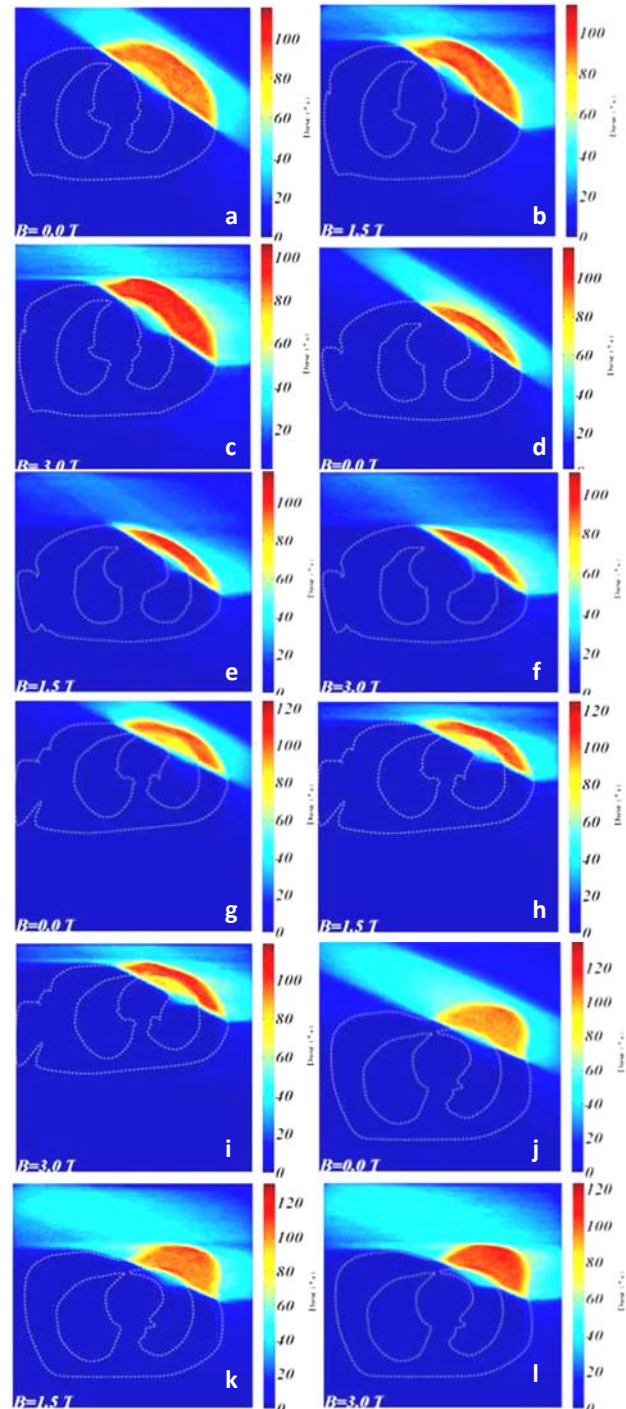


**Figure 4.** Energy deposition in the middle slice of the central plane of patients for different magnetic fields; (a, b and c) patient #1, (d, e and f) patient #2, (g, h and i) patient #3 and (j, k and l) patient #4.

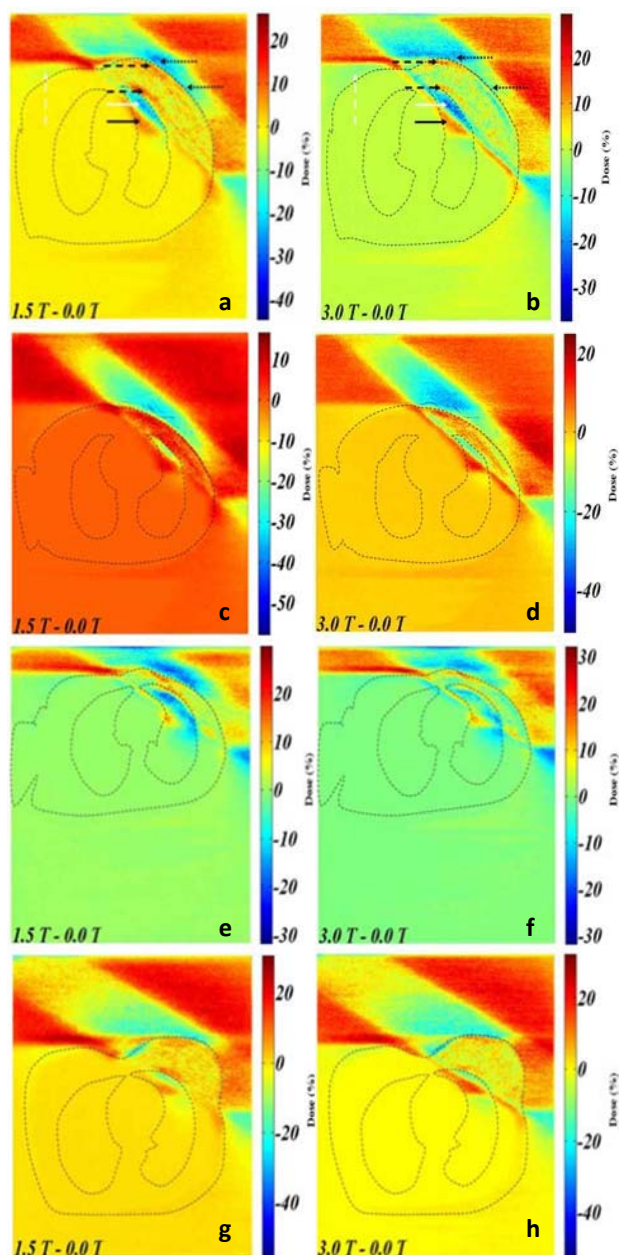


**Figure 5.** Relative dose differences in the middle slice of the central plane at 1.5 and 3.0 T from the zero magnetic field case for (a and b) patient # 1, (c and d) patient # 2, (e and f) patient # 3 and (g and h) patient # 4. Solid white arrows indicate dose reduction in the lung. Dashed black arrows indicate hot spot in the breast. The net effect of the Lorentz force acting on the electrons shifts the dose outside of the patient’s body to the right. Dashed white arrows show dose reduction in the air above the contralateral breast. Solid black arrows indicate the hot spot produced in the lung. Dotted black arrows show dose reduction above the ipsilateral breast.

It is important to note that low density tissues, like lung, were shown to lead to regions of dose decrease in the presence of a conventional magnetic field due to electrons returning to more dense tissues (16,17,25,28,29).

Different maps were drawn to show changes on the dose distribution due to the presence of the magnetic field. At 1.5 and 3 T, hot spot could be observed in the breast, which were indicated by dashed black arrows in the figure, and hot and cold spots in the lung that were indicated by solid black and white arrows, respectively.

In regions near the breast-lung boundaries, the dose was reduced at 1.5 and 3 T with respect to the without magnetic field case, because high-energy charged particles that were scattered from the breast into the lung had a large enough gyration radius for curving back into the breast.

Low-energy charged particles originated far from the breast-lung boundaries in the lung have small gyration radius; therefore, they release their energy in the lung. Furthermore, there are numerous scattered photons on which the magnetic field did not have any influence. Accordingly, the effect of magnetic field reduces in the deeper regions in the lung and the rate of dose reduction decreases to these areas of the lung with respect to regions close to the breast-lung boundaries in the lung (figure 5).

The same scenario takes place at the breast-air boundaries at the entrance of the medial tangent field that causes charge particles curve back into the breast from the air and breast-air boundaries (chest wall skin). Due to the ERE effect, the chest wall skin dose will be reduced (with dotted black arrows shown in figure 5).

For the treatment planning with two opposing beams for the breast, DVHs for the PTV, heart, IL and DAHs for ICWS for different magnetic fields were plotted in figure 6.

As a general trend, the high-dose area of the DVH was seen to be shifted to the right for 1.5 and 3 T with sharp drop of the curve, which was due to the ERE, increasing of the dose to volumes of the breast near the breast-air and breast-lung inside the PTV.

In the IL, figure 6 shows only small changes in the DVHs at 1.5 and 3 T. V20 (where 20 was

expressed as the percentage of the prescription dose) remains reasonably constant. From figure 5, there are obvious changes on the dose distribution within the lung. As the ERE occurs in the breast-lung boundaries, there is highest dose reduction in these areas, in contrast, in regions not close to the breast-lung boundaries, the effect of the magnetic field is reduced and makes some sub-regions hotter.

The ICWS showed good changes in the DAH across the range of the investigated magnetic field strengths. In DVHs of the heart, there is not any significant difference for all patients, but in patient # 3 due to the increase of the dose for the PTV, after re-normalization, noticeable mean dose reduction can be seen (figure 7).

Utilizing magnetic field will help to produce uniform dose distribution to the breast with a sharp DVHs curve for the PTV, however, for the ipsilateral lung and chest wall skin the mean dose was reduced by a mean of 16% and 12% at 1.5 T, and 9% and 7% at 3 T, respectively, depending on different patients and various treatment plan setups.

Two groups studied the effect of the magnetic field on dose distribution in a humanoid phantom in the presence of the strong magnetic field by use of IMRT technique with the help of the Monte Carlo code.

The first group <sup>(29)</sup> investigated the magnetic field effects on dose distribution in the prostate, larynx and oropharynx tissues. They concluded that the presence of a 1.5 T magnetic field does not compromise the ability to achieve the prescribed dose distributions with IMRT.

Other group <sup>(16,17)</sup> investigated lung dosimetry in a linac-MRI radiotherapy unit with a longitudinal magnetic field. The longitudinal configuration exhibited a significant decrease in tissue interface effects and demonstrated an increase in the dose to the PTV as a function of increased magnetic field. The same results were found in our cases with an increase in dose to the PTV.

The CB received a small mean dose giving by a mean (range) of 36 cGy (23-51 cGy) at 0 T. After applying magnetic field of 1.5 and 3 T, the mean dose of CB was reduced by a mean (range)

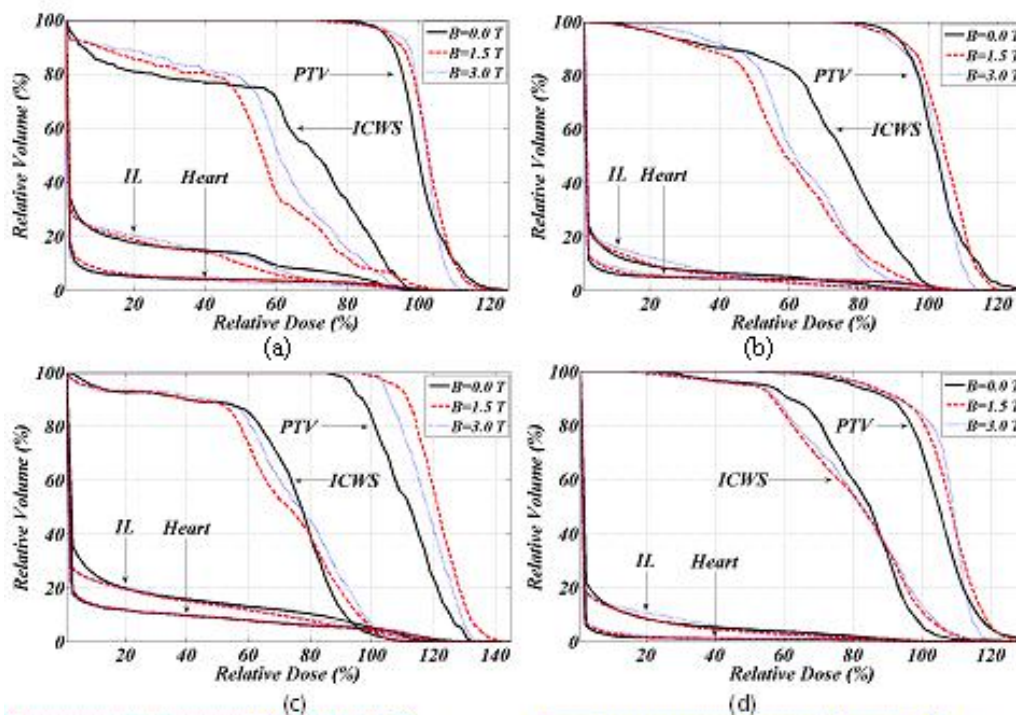


**Figure 6.** Comparison of the breast treatment plan DVHs and DAHs between  $B = 0, 1.5$  and  $3\text{ T}$  in patient # 1 (a), patient # 2 (b), patient # 3 (c) and patient #4 (d). Note that, those volumes within the radiation field are considered for the ICWS DAHs.

of 28% (21-37%) and 48% (32-81%), respectively. There was the same dose reduction to the CCWS by a mean (range) of 58% (44- 75%) and 66% (54-73%) at 1.5 and 3 T. This is explained by the fact that the magnetic field is shown to restrict the lateral spread of secondary electrons to the contralateral organs, resulting in significant dose reductions to the CB and CCWS.

**Dose distribution to the contralateral organs**

It may be assumed that, at the tissue-lung interface and on the chest wall skin to the contralateral, the ERE increases the dose of surrounding tissues; but, the net effect of the Lorentz force acting on the electrons shifts the dose far from the CB (as indicated by dashed white arrow in figure 5).

Mean dose of the CB and internal organs was tabulated in table 3 for the zero magnetic field case. For external beam radiotherapy, the physical wedge compensation technique yielded the largest dose to the neighboring solid organs,

**Table 3.** Mean organ dose of the patients for the zero magnetic field case.

Organs	Mean dose at 0 T (cGy)			
	Patient # 1	Patient # 2	Patient # 3	Patient # 4
CCWS	408	249	166	84
CB	51	33	23	37
CL	18	10	16	11
IL	739	366	786	344
Heart	282	279	605	139

like the IL or the heart. Figure 7 compared the relative mean dose with the selected organs for different magnetic fields with respect to no magnetic field case.

The CB received a small mean dose giving by a mean (range) of 36 cGy (23-51 cGy) at 0 T. After applying magnetic field of 1.5 and 3 T, the mean dose of CB was reduced by a mean (range) of 28% (21-37%) and 48% (32-81%), respectively. There was the same dose reduction to the CCWS by a mean (range) of 58% (44-75%) and 66% (54-73%) at 1.5 and 3 T. This is explained by the fact that the magnetic field is shown to restrict the lateral spread of secondary electrons to the contralateral organs, resulting in significant dose reductions to the CB and CCWS.

Although radiation-induced pneumonitis is considered a trivial issue in most cases of breast radiotherapy, it can be problematic in some patients with unfavorable anatomy and an inadequate radiation technique (33,34). As radiotherapy techniques have improved, the risks of radiation-induced pneumonitis and cardiac complication have declined.

Separate excess relative risks (ERRs) have been reported in patients treated with radiotherapy (35) for breast cancers. Boice (1) found a correlation between the amount of dose to the CB and the likelihood of a secondary malignancy forming. Dasu's competition model projected a continuously increasing risk with dose up to approximately 4-5 Gy followed by a reduced risk in the CB (36). However, using the magnetic field in standard breast radiotherapy for patients with different anatomies and considering the mean dose reduction shown in figure 7, one could clearly conclude the reduction of these complications.

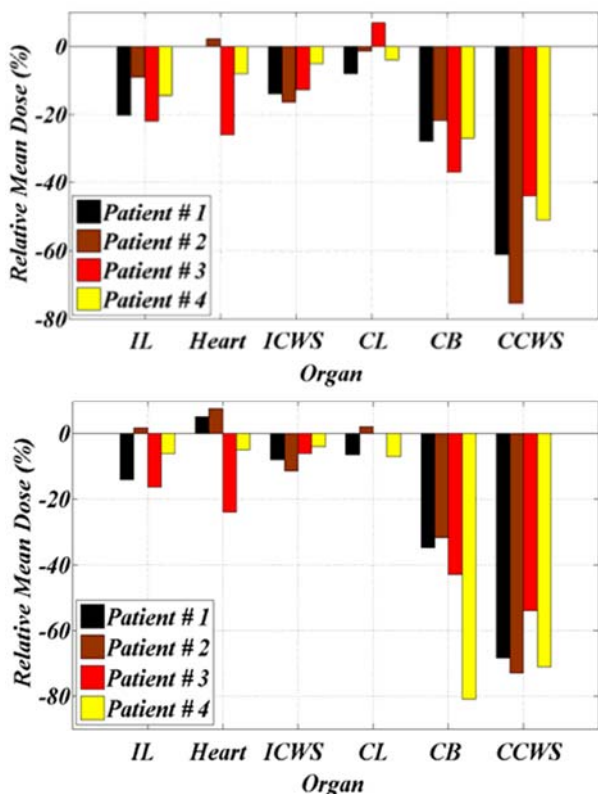


**Figure 7.** Relative mean organ dose variations in all patients at 1.5 T (a) and 3 T (b) with respect to the zero field case.

## CONCLUSIONS

Magnetic field strengths of 1.5 and 3 T were applied in the x direction in the thorax area in which the breast and lung underwent the photon irradiation. The simulations established that the magnetic field can reduce the dose to the internal and contralateral tissues and increase it to the PTV with sharper edge DVH curve. In the all patients, there was noticeable dose reduction to the ICWS, across the range of magnetic field strengths investigated. Therefore, this technique could be more feasible for patients whose skins are not considered a target.

## ACKNOWLEDGEMENT

We are thankful from physicists of radiotherapy departments in Sh. Rajaee and Pars Hospital for their support to proper use of data and planning outputs and special thanks to Mr. Rezaii and Rezazadeh for their kind cooperations.

## REFERENCES

1. Boice JD, Harvey EB, Blettner M, Storall M, Flannery JT (1992) Cancer in the CB after radiotherapy for breast cancer. *N Engl J Med*, **326**: 781-5.
2. Pignol JP, Keller BM, Ravi A (2011) Doses to internal organs for various breast radiation techniques implications on the risk of secondary cancers and cardiomyopathy. *Radi Oncol*, **6**:5-11.
3. Sohn JW, Macklis R, Suh JH, Kupelian P (1999) A mobile shield to reduce scatter radiation to the contralateral breast during radiotherapy for breast cancer: preclinical results. *Int J Radiat Oncol Biol Phys*, **43**: 1037-41.
4. Muller-Runkel R and Kalokhe UP (1994) Method for reducing scatter radiation dose to the contralateral breast during tangential breast irradiation therapy. *Radiology*, **191**:853-5.
5. Macklis RM, Crownover RL, Crowe J, WILoughby T, Sohn J (1999) Reducing scatter radiation to the contralateral breast with a mobile, conformal shield during breast cancer radiotherapy. *Am J Clin Oncol*, **22**:419-25.
6. Hall EJ (2006) Intensity-modulated radiation therapy, protons, and the risk of second cancers. *Int J Radiat Oncol Biol Phys*, **65**: 1-7.
7. Xu XG, Bednarz B, Paganetti H (2008) A review of dosimetry studies on external beam radiation treatment with respect to second cancer induction. *Phys Med Biol*, **53**: R193-241.
8. Shih CC (1975) High energy electron radiotherapy in a magnetic field. *Med Phys*, **2**: 9-13.
9. Chen Y, Bielajew AF, Litzenberg DW, Moran JM, Becchetti FD (2005) Magnetic confinement of electron and photon radiotherapy dose: A Monte Carlo simulation with a nonuniform longitudinal magnetic field. *Med Phys*, **12**: 3810-3818.
10. Pouliot J, Bani-Hashemi A, Chen J, Svatos M, Ghelmansarai F, Mitschke M, Aubin M, Xia P, Morin O, Bucci K, Roach M, Hernandez P, Zheng Z, Hristov D, Verhey L (2005) Low-dose megavoltage cone-beam CT for radiation therapy. *Int J Radiat Oncol Biol Phys*, **61**: 552-560.
11. Nederveen AJ, Dehnad H, Van der Heide UA, Van Moorselaar RJA, Hofman P, Lagendijk JJW (2003) Comparison of megavoltage position verification for prostate irradiation based on bony anatomy and implanted fiducials. *Radiother Oncol*, **68**: 81-8.
12. Lagendijk JJW, Raaymakers BW, Raaijmakers AJE, Overweg J, Brown K J, Kerkhof EM, van der Put RW, Hårdemark B, van Vulpen M, van der Heide UA (2007) MRI/Linac integration. *Radiother Oncol*, doi:10.1016/j.radonc, 10.034.
13. Fallone B, Carlone M, Murray B, Rathee S, Stanescu T, Steciw S, Wachowicz K, Kirkby C (2007) Development of a linac-MRI system for real-time ART. *AAPM Minneapolis 49th Annual Meeting*.
14. Fallone B G, Murray B, Rathee S, Stanescu T, Steciw S, Vidakovic S, Blosser E, Tymofichuk D (2009) First MR images obtained during megavoltage photon irradiation from a prototype integrated linac-MR system. *Med Phys*, **36**: 2084-2088.
15. Kirkby C, Stanescu T, Fallone B G (2009) Magnetic field effects on the energy deposition spectra of MV photon radiation. *Phys Med Biol*, **54**: 243-257.
16. Kirkby C, Murray B, Rathee S, Fallone BG (2010) Lung dosimetry in a linac-MRI radiotherapy unit with a longitudinal magnetic field. *Med Phys*, **37**: 4722-3.
17. Kirkby C, Stanescu T, Rathee S, Carlone M, Murray B, Fallone BG (2008) Patient dosimetry for hybrid MRI-radiotherapy systems. *Med Phys*, **35**: 1019-27.
18. Oborn BM, Metcalfe PE, Butson MJ, Rosenfeld AB (2009) High resolution entry and exit Monte Carlo dose calculations from a linear accelerator 6 MV beam under the influence of transverse magnetic fields. *Med. Phys.* **36**: 3549-59.
19. Oborn BM, Metcalfe PE, Butson MG, Rosenfeld AB, Keall PJ (2012) Electron contamination modeling and skin dose in 6 MV longitudinal field MRIgRT: Impact of the MRI and MRI fringe field. *Med Phys*, **39**: 874-91.
20. Whitmire DP, Bernard DL, Peterson MD (1993) Magnetic Modification of the Electron-dose Distribution in Tissue and Lung Phantoms. *Med Phys*, **5**: 409-17.
21. Bielajew A F (1993) The Effect of Strong Longitudinal

- Magnetic Fields on Dose Deposition From Electron and Photon Beams. *Med Phys*, **20**: 1171-9.
22. Li XA, Reiffel L, Chu J, Naqvi S (2001) Conformal photon-beam therapy with transverse magnetic fields: a Monte Carlo study. *Med Phys*, **28**: 127-33.
  23. Jette D (2000) Magnetic fields with photon beams: dose calculation using electron multiple-scattering theory. *Med Phys*, **27**: 1705-1716.
  24. Raaijmakers A J E, Raaymakers BW, Lagendijk J JW (2008) Magnetic-field-induced dose effects in MR-guided radiotherapy systems: dependence on the magnetic field strength. *Phys Med Biol*, **53**: 909-923.
  25. Raaijmakers AJ, Raaymakers BW, Lagendijk JJ (2005) Integrating a MRI scanner with a 6 MV radiotherapy accelerator: Dose increase at tissue-air interfaces in a lateral magnetic field due to returning electrons. *Phys Med Biol*, **50**: 1363-1376.
  26. Raaymakers BW, Raaijmakers AJ, Kotte AN, Jette D, Lagendijk JJ (2004) Integrating a MRI scanner with a 6 MV radiotherapy accelerator: Dose deposition in a transverse magnetic field. *Phys Med Biol*, **49**: 4109-4118.
  27. Agostinelli, Allison J, Amako Apostolakis J, Araujo H, Arce P, Asai M, Axen D, Banerjee S, Barrand G, Behner F, Bellagamba L, Boudreau J, Broglia L, et al. (2003) GEANT4-a simulation toolkit. *Nucl Instrum Methods Phys Res A*, **506**: 250-303.
  28. Raaijmakers AJE, Raaymakers BW, Lagendijk JJW (2007c) Experimental verification of magnetic field dose effects for the MRI-accelerator. *Phys Med Biol*, **52**: 4283-4291.
  29. Raaijmakers AJE, Hårdemark B, Raaymakers BW, Raaijmakers CPJ, Lagendijk JJW (2007a) Dose optimization for the MRI-accelerator: IMRT in the presence of a magnetic field. *Phys Med Biol*, **52**: 7045-7054.
  30. Sardari D, Maleki R, Samavat H, Esmaeeli A (2010) Measurement of depth-dose of linear accelerator and simulation by use of GEANT4 computer code. *Rep Pract Oncol Radiother*, **15**: 64-68.
  31. The Geant4 web site and Manual, <http://geant4.web.cern.ch/geant4/UserDocUserDocUse/UsersGuides/ForApplication>.
  32. International Commission on Radiation Units and Measurements (1992) Photon, electron, proton and neutron interaction data for body tissues. *Bethesda, MD : ICRU*, report: 46.
  33. Gyenes G, Gagliardi G, Lax I, Fornander T, Rutqvist LE (1997) Evaluation of irradiated heart volumes in stage I breast cancer patients treated with postoperative adjuvant radiotherapy. *J. Clin. Oncol.* **15**: 1348-1353.
  34. Harris EE, Correa C, Hwang WT, Liao J, Litt HI, Ferrari VA, Solin LJ (2006) Late cardiac mortality and morbidity in early -stage breast cancer patients after breast-conservation treatment. *J Clin Oncol*, **24**: 4100- 4106
  35. Travis LB, HIL DA, Dores GM, Gospodarowicz M, van Leeuwen FE, Holowaty E, Glimelius B, Andersson M, Wiklund T, Lynch CF, Van't Veer MB, Glimelius I, Storm H, Pukkala E, Stovall M, Curtis R, Boice JD Jr and Gilbert E (2003) Breast cancer following radiotherapy and chemotherapy among young women with Hodgkin disease. *JAMA*, **290**: 465-475.
  36. Dasu A, Toma-Dasu I, Olofsson J, Karlsson M (2005) The use of risk estimation models for the induction of secondary cancers following radiotherapy. *Acta. Oncol*, **44**: 339-47.